Geophysical Journal International

Geophys. J. Int. (2025) **242,** 1–6
Advance Access publication 2025 May 30
Research Paper

https://doi.org/10.1093/gji/ggaf197

Closing the budget of 20th century true polar wander

Sia Ghelichkhan,[1] Mark J. Hoggard ,[1] Fred D. Richards,[2] Ngai-Ham Chan,[3] Jessica R. Creveling,[4] Kimberley M. Moore[5] and Jerry X. Mitrovica[5]

[1]*Research School of Earth Sciences, Australian National University,* 142 *Mills Rd, Acton ACT* 0200*, Australia. E-mail: siavash.ghelichkhan@anu.edu.au*
[2]*Department of Earth Science and Engineering, Imperial College London, Royal School of Mines, Prince Consort Road, London, SW7 2BP, United Kingdom*
[3]*Helmholtz Centre Potsdam—The GFZ German Research Centre for Geosciences, Wissenschaftspark Albert Einstein, Telegrafenberg,* 14473 *Potsdam, Germany*
[4]*College of Earth, Ocean, and Atmospheric Sciences, Oregon State University, Corvallis,* 97331*, Oregon, USA*
[5]*Department of Earth & Planetary Sciences, Harvard University, Cambridge, Massachusetts 0*2138*, USA*

Accepted 2025 May 19. Received 2025 March 9; in original form 2024 November 12

SUMMARY

We revisit the budget of 20th century true polar wander (∼1°/Myr in the direction of 70°W) using a state-of-the-art adjoint-based reconstruction of mantle convective flow and predictions of ongoing glacial isostatic adjustment that adopt two independent models of Pleistocene ice history. Both calculations are based on a mantle viscosity profile that simultaneously fits a suite of data sets related to glacial isostatic adjustment (Fennoscandian Relaxation Spectrum, post-glacial decay times) and a set of present-day observations associated with mantle convection (long-wavelength gravity-anomalies, plate motions, excess ellipticity of the core–mantle boundary). Our predictions reconcile both the magnitude and direction of the observed true polar wander rate, with convection and glacial isostatic adjustment contributing signals that are 25–30 per cent and ∼75 per cent of the observed rate, respectively. The former assumes that large-scale seismic velocity heterogeneities are purely thermal in origin, and we argue that our estimate of the convection signal likely represents an upper bound due to the neglect of hypothesized compositional variations within the large low-shear velocity provinces in the deep mantle.

Key words: Composition and structure of the mantle; Earth rotation variations; Global change from geodesy; Rheology: Mantle; Dynamics: convection currents and mantle plumes; Dynamics of lithosphere and mantle.

INTRODUCTION

True polar wander (TPW) refers to the long-term motion of the rotation axis of the Earth relative to the surface geography. A combination of astronomic and geodetic measurements indicates that TPW during the 20th century involved a mean drift of the North Pole toward Québec (∼70°W) at a rate of ∼1°/Myr (∼11 cm yr^{-1}; Argus & Gross 2004). Beginning in the early 1980s, this signal was assumed to reflect the ongoing adjustment of the Earth in response to the past ice age—a hypothesis consistent with the observed direction of the polar motion—and models of the glacial isostatic adjustment (GIA) process were compared to the observed rate to infer deep mantle viscosity (e.g. Sabadini & Peltier 1981; Sabadini *et al.* 1982; Wu & Peltier 1984).

It was soon recognized that modern climate signals, and particularly the melting of glacier systems, could have a non-negligible impact on TPW (e.g. Peltier 1988) and studies of this connection came to define 'Munk's Enigma'. Munk (2002) demonstrated that various observations related to Earth rotation, including TPW, could be reconciled with a standard GIA model, leaving no room for the signal associated with modern glacier or ice sheet melting at a rate implied by estimates of global mean sea level (GMSL) rise over the 20th century. Mitrovica *et al.* (2015) resolved this enigma by adopting an updated (and lower) estimate of 20th century GMSL rise (Hay *et al.* 2015), using an improved model of the radial profile of mantle viscosity, and a more accurate treatment of GIA-induced TPW (Mitrovica *et al.* 2005). Their analysis concluded that GIA was the dominant signal in 20th century TPW, explaining the direction and ∼80 per cent of the rate of polar motion.

These various studies neglected the possibility that mantle convective flow, the driving force of plate tectonics, contributed significantly to the TPW over the past century. Steinberger & O'Connell (1997), in contrast, concluded that convection contributed ∼40 per cent of the modern TPW rate in the direction of East Greenland, and argued that the signal should be considered in efforts to close the budget of 20th century TPW. Their study used backward in time advection of a model of present-day mantle density heterogeneity inferred from seismic tomography spanning tens of millions

of years (ignoring thermal diffusion) to establish time-series of inertia tensor perturbations. Using the same viscous flow theory, but different models for the mantle density field that combined reconstructions of plate subduction history with density anomalies associated with the two Large Low Shear Velocity Provinces (LLSVPs) in the deep mantle, Steinberger & Torsvik (2010) estimated TPW rates of 0–0.3°/Myr over the past 10 Myr, generally in the direction of Greenland. These efforts were part of a large body of published work that explored the relatively muted (∼10°) history of TPW over the past 120 Myr inferred from paleomagnetic data using a range of rotational stability theories (Ricard *et al.* 1993; Richards *et al.* 1997, 1999; Greff-Lefftz 2004; Steinberger & Torsvik 2008; Rouby *et al.* 2010; Chan *et al.* 2011). A general conclusion from such studies was that long-term rates of TPW in recent geological history were of order 0.1°/Myr (∼1.1 cm yr^{-1}).

Adhikari *et al.* (2018) revisited the budget of 20th century TPW considering contributions from GIA, modern melting of ice sheets and glaciers, water impoundment in dams, flux of groundwater between continents and oceans, steric- and seismogenic effects and mantle convection (see below). They concluded that a mantle convection signal in TPW with a magnitude of ∼50–70 per cent of the observed rate was necessary to reconcile the 20th century trend after correction for the remaining signals. The analysis involved 283 convection simulations using a variety of approaches, including a tracking of inertia tensor perturbations based on reconstructions of subduction histories or backward advection of initial buoyancy fields computed from a suite of seismic tomography models. The simulations had a mean TPW rate of 0.21° ± 0.01°/Myr, significantly lower than the above range (i.e. lower than 50–70 per cent of observed), and only 5 of the predictions yielded a convection signal that satisfied the TPW observation. The study also concluded that GIA contributed only ∼30 per cent of the observed 20th century rate.

Rigorously establishing the magnitude of the mantle convection signal in 20th century TPW and closing the budget of the observed signal is important for efforts to use the datum to constrain modern global change processes. Towards this end, we revisit the issue here using a new simulation of mantle convection across the Cenozoic based on an adjoint methodology that solves the full field equations governing compressible mantle convection, including thermal diffusion (Ghelichkhan & Bunge 2016, 2018; Ghelichkhan *et al.* 2021, 2024). Adjoint modelling avoids transient behaviour that can occur in backward advection schemes—behaviour that can contaminate the most recent phase of evolution, which is the time-period of interest here. A second improvement over previous analyses is the rotational stability theory we apply to track TPW. Previous studies generally adopted the canonical TPW theory of Gold (1955) and Goldreich & Toomre (1969) in which no stabilization of the rotation axis due to delayed adjustment of the rotational bulge of the Earth is included. Our calculations are based on the treatment of Moore *et al.* (2017), which includes this stabilization due to the rotational bulge (Ricard *et al.* 1993) and the so-called 'remnant bulge' (Willemann 1984; Matsuyama *et al.* 2006) associated with the presence of a (high viscosity) viscoelastic lithosphere.

BACKGROUND

Adjoint based reconstructions of cenozoic mantle dynamics and structure

Our reconstructions of mantle heterogeneity evolution are based on the methodology detailed by Ghelichkhan *et al.* (2021). The adjoint method generates an optimized trajectory of global mantle flow by iteratively refining the initial temperature field to minimize a cost function measuring the difference between the model-predicted temperature field at present day and an inferred present-day field derived from seismic tomography. Unlike backward advection schemes, which simulate backward evolution by reversing the gravitational direction, leading to diffusion that operates independently of gravity's orientation, our approach treats the problem as an optimization task. This reframing prevents the unrealistic diffusive artefacts typical in backward advection schemes. Nonetheless, the iterative nature of the method is computationally intensive, requiring hundreds of thousands of CPU hours, far exceeding the resources typical of conventional forward-time models.

In this study, we adopt the MF-SL reconstruction of Ghelichkhan *et al.* (2021), which employs the viscosity profile of Mitrovica & Forte (2004). This reconstruction retrodicts mantle heterogeneity, and the associated non-hydrostatic inertia tensor perturbations, since 50 Ma under a purely thermal interpretation, using high-resolution global models with ∼670 million finite elements to capture mantle dynamics at Earth-like flow regimes. The present-day seismic structure is inferred from the shear wave speed model of SEMUCB-WM1 (French & Romanowicz 2014), with additional refinement in the uppermost 300 km using the vertically polarized shear speed model SL2013sv (Schaeffer & Lebedev 2013). Temperature conversions account for both elastic and anelastic effects, using a thermodynamically consistent pyrolitic mantle mineralogy model and a profile for the mantle quality factor Q as outlined in Ghelichkhan *et al.* (2021).

Rotational stability theory

With few exceptions, predictions of TPW driven by mantle convection adopt the equilibrium (i.e. final state) theory of Gold (1955) and Goldreich & Toomre (1969) in which there is no long-term stabilization of the Earth's rotation axis (e.g. Adhikari *et al.* 2018). Ricard *et al.* (1993) extended the rotational equilibrium (i.e. final state) theory of Gold (1955) and Goldreich & Toomre (1969) to incorporate time dependence in TPW associated with the delayed, viscoelastic adjustment of the rotational bulge. This rotational stability theory has been extended further to incorporate a stabilization mechanism (the so-called 'remnant bulge') first described by Willemann (1984) associated with stresses in an elastic lithosphere that arise from the adjustment of the bulge (Matsuyama *et al.* 2006; Creveling *et al.* 2012; Harada 2012; Chan *et al.* 2014). These elastic stresses introduce a memory of an initial pole position. An additional extension, by Moore *et al.* (2017), treats the case of a viscoelastic lithosphere. On timescales much shorter than the viscous relaxation time of the lithosphere, the polar motion computed using the Moore *et al.* (2017) theory follows the elastic lithosphere case, whereas on timescales much longer than the relaxation time of the lithosphere, the calculations converge to those computed using the time-dependent stability theory of Ricard *et al.* (1993).

Our calculations of convection-induced TPW are based on the treatment of Moore *et al.* (2017; eq. 12). All Earth models adopt the elastic and density structure of the seismic Preliminary Reference Earth Model (Dziewonski & Anderson 1981) and the viscosity profile shown in Fig. 1 (Mitrovica *et al.* 2015; henceforth M2015), which is characterized by an ∼2.5 order of magnitude increase from the base of the lithosphere to the deep mantle, followed by a decrease of comparable amount toward the core–mantle boundary (CMB). The profile is within the class of models derived

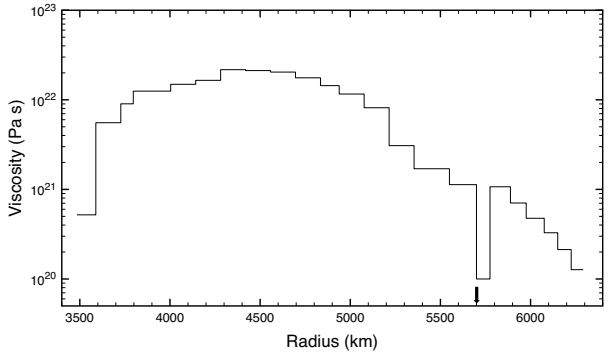

Figure 1. Mantle viscosity profile adopted in simulations. 23-layer viscosity profile extending from the core–mantle boundary to the base of the 80 km thick lithosphere, after Mitrovica *et al.* (2015). Arrow on the *x*-axis indicates the depth of the boundary between upper and lower mantle.

through simultaneous inversion of ice age and mantle convection data sets (Mitrovica & Forte 2004). The ice age data included a set of observations that are relatively insensitive to uncertainties in ice history, the Fennoscandian Relaxation Spectrum and post-glacial decay times over Hudson Bay and Fennoscandia. The convection data included long-wavelength gravity-anomalies, plate motions, surface dynamic topography and the excess ellipticity of the CMB. We consider three variations of this structure distinguished based on the adopted viscosity of the lithosphere (10^{25}, 10^{26}, and 10^{27} Pa s) which establishes the relaxation time of the lithosphere—and thus the timescale over which any reorientation of the rotation axis is stabilized by the remnant bulge in the presence of the convective driving force. In all cases the lithospheric thickness is 80 km.

The TPW calculations extend 3000 Myr and begin with a 2950 Myr ramp-up in which the inertia tensor stays fixed to the first values computed in the adjoint simulation. The calculations end at the present day. TPW reconstructions adopt the same viscosity profile used in the adjoint simulation and, in addition, we consider three values for lithospheric viscosity: 10^{25}, 10^{26} and 10^{27} Pa s. These values have characteristic (Maxwell) relaxation times of 5, 50 and 500 Myr, respectively, and the 2950 Myr ramp-up ensures that the pole position at 50 Ma is the same (i.e. viscous effects have fully relaxed) in all three cases.

Modern drivers of TPW

Fig. 2 shows both the observational constraint on TPW (Argus & Gross 2004; black oval—solid) and the signal associated with the impact of a suite of processes thought to drive TPW. The signal shown by the red oval involves contributions from: (1) modern ice mass flux from global glacier systems, the Greenland Ice Sheet, and the Antarctic Ice Sheet; (2) water impoundment in dams; (3) flux of groundwater between continents and oceans; (4) ocean steric effects; and (5) seismic events. We adopt values Adhikhari *et al.* (2018) cited for each of these signals except for water impoundment where our analysis of the TPW signal is based on the extensive database of Hawley *et al.* (2020). The modern ice mass signal (1), which dominates the total, was based on the Randolph Glacier Inventory (Marzeion *et al.* 2015; RGI Consortium 2017) derived from climate modelling consistent with observations of glacier volume change and surface mass balance, 20th century Greenland Ice Sheet mass changes estimated from aerial imagery and altimetry measurements (Kjeldsen *et al.* 2015), and a suite of regional studies of 20th century Antarctic Ice Sheet and glacier changes. The signal from groundwater flux was based on Wada *et al.* (2012), steric effects on Landerer *et al.* (2009). Finally, the polar wander signal from co- and interseismic deformation was taken from Cambiotti *et al.* (2016). The components (2)–(4) yield a net signal of ∼0.3 cm yr^{-1} with an uncertainty of ∼1 cm yr^{-1}. We henceforth term the total signal from (1)–(5) the modern ice flux + signal.

RESULTS

The predicted pole path since 50 Ma (i.e. from the onset on convection-induced perturbations in the inertia tensor) is broadly similar in all three cases and, as one would expect, the net displacement of the pole decreases as the lithospheric viscosity increases (Fig. 3). The relaxation time of the 10^{25} Pa s lithosphere is sufficiently short that any further decrease in viscosity will not impact the pole path (i.e. stabilization is provided by the rotational bulge alone). In contrast, the highest lithospheric viscosity case experiences negligible viscous relaxation in the lithosphere over the 50-Myr convection simulation, and the lithosphere behaves essentially as an elastic plate (i.e. stabilization is also provided by the remnant bulge). The computed path approximately follows the meridian −135°E/45°E from ∼50–15 Ma, and then turns to follow a southwest path over the subsequent 15 Myr. The present-day TPW rate in these convection simulations increases from 3.3 to 3.9 cm yr^{-1} (3.0–3.5°/Myr) as the lithospheric viscosity is decreased from 10^{27} to 10^{25} Pa s, a range that represents ∼25–30 per cent of the observed magnitude (Fig. 2; green oval). Since stabilization by the remnant bulge is small for lithospheric viscosities less than 10^{25} Pa s, any further reduction in this viscosity toward the value in the shallow upper mantle (∼10^{20} Pa s) has negligible effect on the predicted rate. In these TPW calculations we have neglected the impact of breaks in the lithosphere (i.e. plate boundaries) which would weaken stabilization by the remnant bulge (Creveling *et al.* 2012). The prediction in the case of the 10^{27} Pa s lithosphere would—if breaks were incorporated—move toward the low viscosity prediction, but the latter would still serve as a bound on the predicted path.

The final pole positions in the three TPW time-series are not coincident with the present-day pole (Fig. 3). Steinberger & O'Connell (1997) and Adhikari *et al.* (2018) enforced a present-day pole position by adding a constant shift in the geopotential to match the present-day position. This approach imposes a fixed perturbation to the inertia tensor across the entire time-series. A more rigorous approach would be to run many adjoint-based convection simulations and search for the subset that predict a present-day pole position 'closest' to the observed location but given the numerical cost of doing so (see Background) we leave this effort to future work. Nevertheless, the displacement of the predicted present-day pole positions in Fig. 3 from the observed location are relatively small (e.g. less than 6° for a lithospheric viscosity of 10^{27} Pa s).

We turn next to TPW driven by GIA. Ongoing polar wander (or motion) associated with remnant isostatic adjustment following the last ice age is sensitive to the broad geographic distribution of ice mass flux and its evolution from the Last Glacial Maximum (LGM) to the Holocene. To explore the uncertainty associated with history, we consider predictions of TPW based on the M2015 viscosity model (Fig. 1) and three independent, global models of ice history across the last glacial cycle, ICE-6 G (Peltier *et al.* 2015), ICE-7 G (Roy & Peltier 2018) and a model developed at the Australian National University (ANU) (Lambeck *et al.* 2014). In addition,

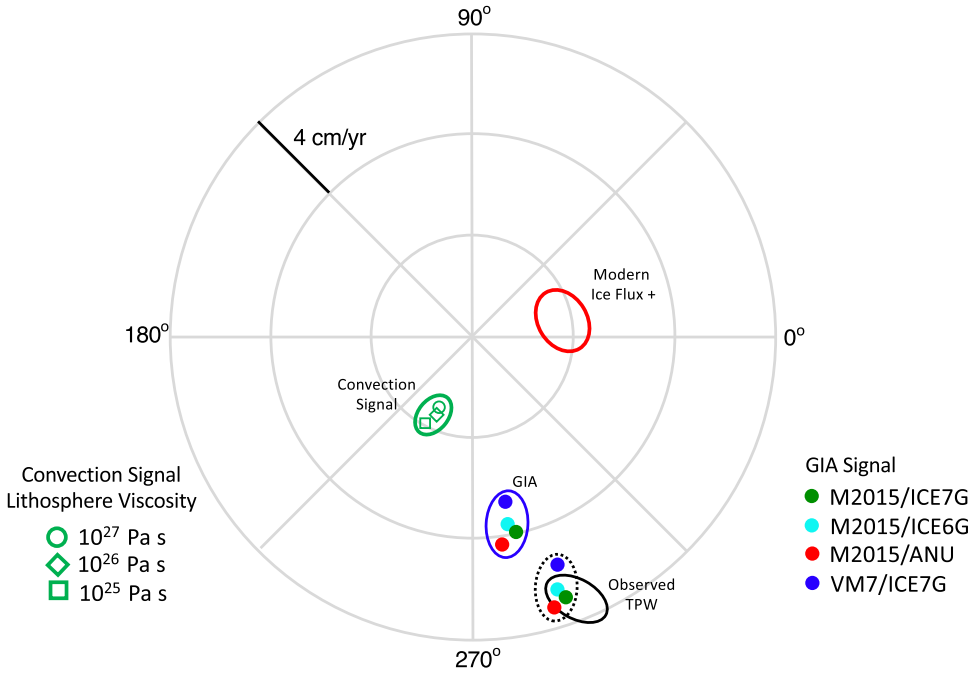

Figure 2. Observed and predicted 20th century TPW. Black oval (solid line)—observed TPW based on results in Argus & Gross (2004) using the hotspot or mean mantle reference frames. The modern ice flux+, mantle convection and GIA signals are described in the text. Uncertainties in each signal are shown as red, green and blue ovals, respectively. Four GIA simulations distinguished based on the adopted ice history (as labelled, bottom right) are shown. The convection predictions involve three reconstructions distinguished based on the viscosity of the lithosphere (as labelled, bottom left). Black oval (dotted line)—combination of modern ice flux+, convection and GIA signals. The oval is positioned by shifting the blue GIA oval using the centroid of the modern ice flux + and convection ovals. Angles on the perimeter refer to degrees, east longitude.

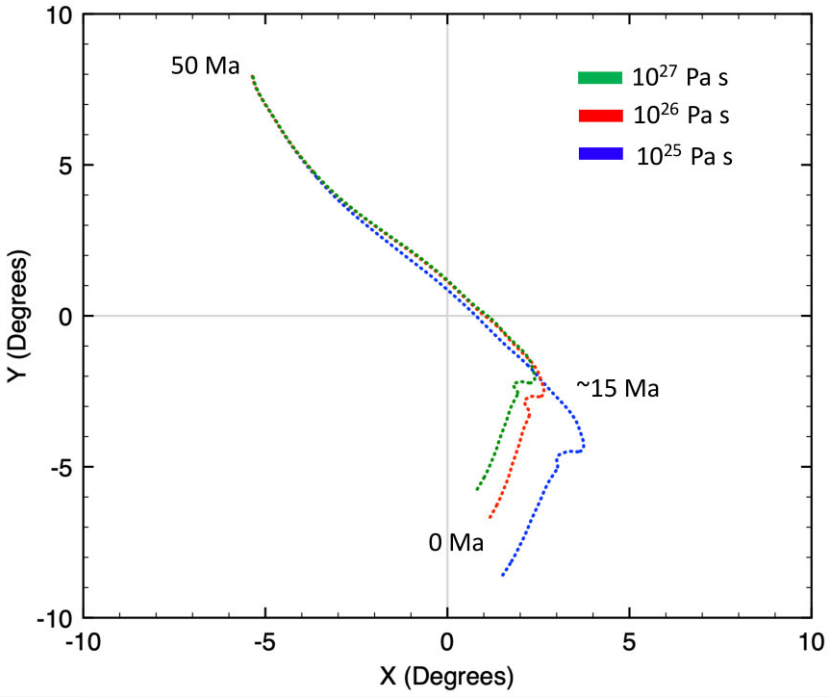

Figure 3. Predicted convection-driven TPW paths. Results are shown for TPW calculations in which the adopted viscosity of the lithosphere is varied (as labelled). The path is shown for a Cartesian coordinate system centred on the north pole in which *X* and *Y* axes are in the directions of 0°E and 90°E. Calculations with higher lithospheric viscosity are marked with shorter TPW paths.

we have also considered the combination of the ICE-7 G history and the VM7 viscosity profile to which it is coupled. The VM7 viscosity model differs from earlier models from the same group by increasing the deep mantle to a value of $\sim 10^{22}$ Pa s, consistent with inferences of Mitrovica & Forte (2004), Mitrovica *et al.* (2015) and Lau *et al.* (2016). The last of these studies demonstrated that a deep

mantle viscosity in this range is necessary to reconcile satellite-derived constraints on the rate of present-day rate of change of the degree-2 zonal harmonic of the Earth's geopotential.

Predictions of the present-day TPW signal due to GIA based on the above models and the rotational stability theory of Mitrovica *et al.* (2005) are shown in Fig. 2 (green, cyan, red and blue solid circles within the blue oval). The timescale of ice age loading is faster than the decay time of the lowest-viscosity lithosphere considered in the convection simulations (as noted above, ∼5 Myr for the case of 10^{25} Pa s), and thus calculations based on any of the viscoelastic lithospheres are essentially identical. The GIA predictions are relatively insensitive to the choice of ice history and the fine-scale details of mantle viscosity. The four calculations yield magnitudes that are ∼70 per cent of the observed TPW rate with a direction of ∼75–80°W, that is, toward the location of the Laurentide Ice Sheet that dominated the excess ice budget at LGM. Moreover, the sum of the modern ice flux+, convection and GIA signals—shown by the dashed black oval—falls within (and thus close the budget of) the observed 20th century rate. As a final note, we also considered the combination of the Lau *et al.* (2016) viscosity model and all three of the ice histories listed above (ICE-6 G, ICE-7 G and ANU) and the results differed by less than 6 per cent from the analogous series based on the M2015 viscosity model.

CONCLUSIONS

We conclude that the signal of ongoing GIA dominates the budget of modern TPW and that mantle convection-induced TPW contributed 25–30 per cent of the observed rate. The latter confirms the argument of Steinberger & O'Connell (1997) that the signal is a non-negligible component of the 20th century budget, and while it is relatively consistent with the mean TPW rate of the large suite of predictions in Adhikari *et al.* (2018) it is well below the subset they used to close the TPW budget.

Convection-induced TPW is governed by long-wavelength deep mantle buoyancy structure, and particularly the density anomalies associated with the two LLSVPs at the base of the mantle below southern Africa and the southwest Pacific (e.g. Ritsema *et al.* 2011; McNamara 2019; Richards *et al.* 2023). Our mapping of seismic to density heterogeneity assumes that the former is due to purely temperature effects, but there is evidence that these structures involve significant compositional heterogeneity (e.g. Forte & Mitrovica 2001; Lau *et al.* 2017; Richards *et al.* 2023), and in this case we have likely overestimated the buoyancy of the LLSVPs. Thus, we interpret our estimate of the convection signal in TPW to be an upper bound. Indeed, a reduction of this signal by a factor of two, consistent with long-term rates of TPW (Greff-Lefftz 2004; Rouby *et al.* 2010; Chan *et al.* 2011), can be accommodated while preserving a fit to the observed 20th century rate. In future work we will extend the convection analysis described herein to incorporate the influence of compositional heterogeneities within an adjoint methodology (Ghelichkhan & Bunge 2018) and to run a larger set of such simulations.

ACKNOWLEDGMENTS

We thank the Editor, Dr Kosuke Heki, and two anonymous reviewers for their constructive comments on an earlier version of this manuscript. During the review phase we became aware of a preprint by Alessandro Forte and colleagues (https://www.researchsquare.com/article/rs-5397333/v1) that considers TPW over the past 70 Myr using a distinct reconstruction methodology and arrives at a consistent conclusion regarding the present-day rate of TPW contributed by mantle convection.

Funding: SG and MJH were both supported by the Australian Research Council via Discovery Early Career Researcher Awards (DE250100663, DE220101519). MH was also supported by Geoscience Australia. JXM was supported by Harvard University and the MacArthur Foundation.

DATA AVAILABILITY

Results described in this paper are available via request to the authors.

REFERENCES

Adhikari, S., Caron, L., Steinberger, B., Reager, J.T., Kjeldsen, K.K., Marzeion, B., Larour, E. & Ivins, E.R., 2018. What drives 20th century polar motion?, *Earth planet. Sci. Lett.,* **502,** 126–132.

Argus, D.F. & Gross, R.S., 2004. An estimate of motion between the spin axis and the hotspots over the past century, *Geophys. Res. Lett.,* **31,** L06614.

Cambiotti, G., Wang, X., Sabadini, R. & Yuen, D., 2016. Residual polar motion caused by coseismic and interseismic deformations from 1900 to present, *Geophys. J. Int.,* **205,** 1165–1179.

Chan, N.-H., Mitrovica, J.X., Daradich, A., Creveling, J.R., Matsuyama, I. & Stanley, S., 2014. Time-dependent rotational stability of dynamic planets with elastic lithospheres, *J. Geophys. Res.—Planets,* **119,** 169–188.

Chan, N.-H., Mitrovica, J.X., Matsuyama, I., Latychev, K., Creveling, J.R., Stanley, S. & Morrow, E., 2011. The rotational stability of a convecting Earth: the Earth's figure and TPW over the last 100 myr, *Geophys. J. Int.,* **187,** 773–782.

Creveling, J.R., Mitrovica, J.X., Chan, N.-G., Latychev, K. & Matsuyama, I., 2012. Mechanisms for oscillatory true polar wander, *Nature,* **491,** 244–248.

Dziewonski, A.W. & Anderson, D., 1981. Preliminary Reference Earth Model, *Phys. Earth planet. Inter.,* **25,** 297–356.

Forte, A.M. & Mitrovica, J.X., 2001. High viscosity deep mantle flow and thermochemical structure inferred from seismic and geodynamic data,", *Nature,* **410,** 1049–1056.

French, S.W. & Romanowicz, B.A., 20014. Whole-mantle radially anisotropic shear velocity structure from spectral-element waveform tomography, *Geophys. J. Int.,* **199,** 1303–1327.

Ghelichkhan, S. & Bunge, H.-P., 2018. The adjoint equations for thermochemical compressible mantle convection: derivation and verification by twin experiments, *Proc. R. Soc. A,* **474,** 20 180 329.

Ghelichkhan, S. & Bunge, H.-P., 2016. The compressible adjoint equations in geodynamics: derivation and numerical assessment, *Int. J. Geomath.,* **7,** 1–30.

Ghelichkhan, S., Bunge, H.-P. & Oeser, J., 2021. Global mantle flow retrodictions for the early Cenozoic using an adjoint method: evolving dynamic topographies, deep mantle structures, flow trajectories and sublithospheric stresses, *Geophys. J. Int.,* **226,** 1432–1460.

Ghelichkhan, S., Gibson, A., Davies, D.R., Kramer, S.C. & Ham, D.A., 2024. Automatic adjoint-based inversion schemes for geodynamics: reconstructing the evolution of Earth's mantle in space and time, *Geosci. Model. Dev.,* **17**(13), 5057–5086.

Gold, T., 1955. Instability of the Earth's axis of rotation, *Nature,* **175,** 526–529.

Goldreich, P. & Toomre, A., 1969. Some remarks on polar wandering, *J. geophys. Res.,* **74,** 2555–2567.

Greff-Lefftz, M., 2004. Upwelling plumes, superswells and true polar wander, *Geophys. J. Int.,* **159,** 1125–1137.

Harada, Y., 2012. Long-term polar motion on a quasi-fluid planetary body with an elastic lithosphere: semi-analytic solutions of the time-dependent equation, *Icarus,* **220,** 449–465.

Hawley, W.B., Hay, C.C., Mitrovica, J.X. & Kopp, R.E., 2020. A spatially variable time-series of sea level change due to artificial water impoundment, *Earth's Future,* **8,** e2020EF001497.

Hay, C.C., Morrow, E., Kopp, R.E. & Mitrovica, J.X., 2015. Probabilistic reanalysis of twentieth-century sea-level rise, *Nature,* **517,** 481–484

Kjeldsen, K. *et al.*, 2015. Spatial and temporal distribution of mass loss from the Greenland Ice Sheet since AD 1900, *Nature,* **528,** 396–400.

Lambeck, K., Rouby, H., Purcell, A., Sun, Y. & Sambridge, M., 2014. Sea level and global ice volumes from the Last glacial Maximum to the holocene, *Proc. Natl. Acad. Sci. USA.,* **111,** 15 296–15 303.

Landerer, F., Jungclaus, J. & Marotzke, J., 2009. Long-term polar motion excited by ocean thermal expansion, *Geophys. Res. Lett.,* **36,** L17603.

Lau, H.C.P., Mitrovica, J.X., Austermann, J., Crawford, O., Al-Attar, D. & Latychev, K., 2016. Inferences of mantle viscosity based on ice age data sets: radial structure, *J. Geophys. Res. Solid Earth,* **121,** 6991–7012.

Lau, H.C.P., Mitrovica, J.X., Davis, J.L., Tromp, J., Yang, H.-Y. & Attar, D., 2017. Tidal tomography constrains Earth's deep mantle buoyancy, *Nature,* **551,** 321–326.

Marzeion, B., Laclercq, P., Cogley, J. & Jarosch, A., 2015. Brief communication: global reconstructions of glacier mass change during the 20th century are consistent, *Cryosphere,* **9,** 2399–2404.

Matsuyama, I., Mitrovica, J.X., Perron, J.T., Manga, M. & Richards, M.A., 2006. Rotational stability of dynamic planets with elastic lithospheres, *J. geophys. Res.,* **111,** 1–18.

McNamara, A.K., 2019. A review of large low shear velocity provinces and ultra low velocity zones, *Tectonophysics,* **760,** 199–220.

Mitrovica, J.X. & Forte, A.M., 2004. A new inference of mantle viscosity based upon joint inversion of convection and glacial isostatic adjustment data, *Earth planet. Sci. Lett.,* **225,** 177–189.

Mitrovica, J.X., Hay, C.C., Morrow, E., Kopp, R.E., Dumberry, M. & Stanley, S., 2015. Reconciling past changes in Earth rotation with 20th century global sea-level rise: resolving Munk's enigma, *Sci. Adv.,* **1,** e1500679, doi: 10.1126/sciadv.1500679.

Mitrovica, J.X., Wahr, J.M., Matsuyama, I. & Paulson, A., 2005. The rotational stability of an ice-age Earth, *Geophys. J. Int.,* **161,** 491–506.

Moore, K., Chan, N.-H., Daradich, A. & Mitrovica, J.X., 2017. Time dependent rotational stability of planets with viscoelastic lithospheres, *Icarus,* **289,** 34–41.

Munk, W., 2002. Twentieth century sea level: an enigma, *Proc. Natl. Acad. Sci. USA,* **99,** 6550–6555.

Peltier, W.R., 1988. Global sea level and Earth rotation, *Science,* **240,** 895–891.

Peltier, W.R., Argus, D.F. & Drummond, R., 2015. Space geodesy constrains ice age terminal deglaciation: the global ICE-6G_C (VM5a) model, *J. Geophys. Res. Solid Earth,* **120,** 450–487.

RGI Consortium, 2017. *Randolph Glacier Inventory—A Dataset of Global Glacier Outlines: Version 6.0: Technical Report, Global Land Ice Measurements from Space,* Colorado, USA. Digital Media.

Ricard, Y., Spada, G. & Sabadini, R., 1993. Polar wandering of a dynamic Earth, *Geophys. J. Int.,* **113,** 284–298.

Richards, F.D., Hoggard, M.J., Ghelichkhan, S., Koelemeijer, P. & Lau, H.C.P., 2023. Geodynamic, geodetic, and seismic constraints favour deflated and dense-cored LLVPs, *Earth planet. Sci. Lett.,* **60,** 117 964.

Richards, M.A., Bunge, H.-P., Ricard, Y. & Baumgardner, J.R., 1999. Polar wandering in mantle convection models, *Geophys. Res. Lett.,* **26,** 1777–1780.

Richards, M.A., Ricard, Y., Lithgow-Bertelloni, C., Spada, G. & Sabadini, R., 1997. An explanation for Earth's long-term rotational stability, *Science,* **275,** 372–375.

Ritsema, J., Deuss, A., van Heijst, H.J. & Woodhouse, J.H., 2011. S40RTS: a degree-40 shear-velocity model for the mantle from new Rayleigh wave dispersion, teleseismic traveltime and normal-mode splitting function measurements, *Geophys. J. Int.,* **184,** 1223–1236.

Rouby, H., Greff-Lefftz, M. & Besse, J., 2010. Mantle dynamics, geoid, inertia and TPW since 120 myr, *Earth planet. Sci. Lett.,* **292,** 301–311.

Roy, K. & Peltier, W.R., 2018. Relative sea level in the Western Mediterranean basin: a regional test of the ICE-7GNA (VM7) model and a constraint on late holocene antarctic deglaciation, *Quat. Sci. Rev.,* **183,** 76–87.

Sabadini, R. & Peltier, W.R., 1981. Pleistocene deglaciation and the Earth's rotation: implications for mantle viscosity, *Geophys. J. R. Astron. Soc.,* **66,** 553–578.

Sabadini, R., Yuen, D.A. & Boschi, E., 1982. Polar wandering and the forced responses of a rotating, multilayered, viscoelastic planet, *J. geophys. Res.,* **87,** 2885.

Schaeffer, A.J. & Lebedev, S., 2013. Global shear speed structure of the upper mantle and transition zone, *Geophys. J. Int.,* **194,** 417–449.

Steinberger, B. & O'Connell, R.J., 1997. Changes of the Earth's rotation axis owing to the advection of mantle density anomalies, *Nature,* **387,** 169–173.

Steinberger, B. & Torsvik, T.H., 2008. Absolute plate motions and true polar wander in the absence of hotspot tracks, *Nature,* **452,** 620–623.

Steinberger, B. & Torsvik, T.H., 2010. Toward an explanation for the present and past locations of the poles, *Geochem. Geophys. Geosyst.,* **11,** doi: 10.1029/2009GC002889.

Wada, Y., van Beek, L., Weiland, F., Chao, B., Wu, Y. & Bierkens, M., 2012. Past and future contribution of global groundwater depletion to sea-level rise, *Geophys. Res. Lett.,* **39,** L09402.

Willemann, R.J., 1984. Reorientation of planets with elastic lithospheres, *Icarus,* **60,** 701–709.

Wu, P. & Peltier, W.R., 1984. Pleistocene deglaciation and the Earth's rotation: a new analysis, *Geophys. J. R. Astron. Soc.,* **76,** 753–791.